(c)2002 American Institute of Aeronautics & Astronautics or Published with Permission of Author(s) and/or Author(s)' Sponsoring Organization.

A02-13583

AIAA 2002-0260

Adaptive Aerodynamic Optimization of Regional Jet Aircraft

B.I. Soemarwoto
National Aerospace Laboratory NLR, The Netherlands

M. Laban
National Aerospace Laboratory NLR, The Netherlands

A. Jameson
Stanford University, U.S.A.

A.L. Martins
Empresa Brasileira de Aeronáutica S.A., Brasil

B. Oskam
National Aerospace Laboratory NLR, The Netherlands

40th AIAA Aerospace Sciences Meeting and Exhibit
January 14–17, 2002/Reno, NV

For permission to copy or republish, contact the American Institute of Aeronautics and Astronautics 1801 Alexander Bell Drive, Suite 500, Reston, VA 20191–4344

(c)2002 American Institute of Aeronautics & Astronautics or Published with Permission of Author(s) and/or Author(s)' Sponsoring Organization.

Adaptive Aerodynamic Optimization of Regional Jet Aircraft

B.I. Soemarwoto *
National Aerospace Laboratory NLR, The Netherlands
M. Laban *
National Aerospace Laboratory NLR, The Netherlands
A. Jameson †
Stanford University, U.S.A.
A.L. Martins ‡
Empresa Brasileira de Aeronáutica S.A., Brasil
B. Oskam §
National Aerospace Laboratory NLR, The Netherlands

Nomenclature

A	cross-sectional area
$\mathcal{A}$	aerodynamic constraint functional
C	curvature
C_D	total drag coefficient
C_l	sectional lift coefficient
C_m	sectional pitching moment coefficient
$\bar{C}_p$	normalized pressure coefficient
$\bar{C}_{dw}$	normalized wave drag coefficient
$\bar{C}_{dv}$	normalized viscous drag coefficient
$\vec{\mathbf{F}}$	flux vector
$\mathcal{G}$	geometric constraint
H	3D boundary layer shape factor
M	Mach number
$\mathcal{P}$	aerodynamic objective functional
$\mathbf{Q}$	conservative flow variables
R_{LE}	leading edge radius
Re	Reynolds number
$\mathbf{W}$	flow condition parameters
b	wing span
n_a	number of aerodynamic constraints
n_p	number of aerodynamic objectives
n_f	number of design point
n_g	number of geometric constraints
t/c	thickness ratio
x, y, z	Cartesian axes
δ_{TE}	trailing edge included angle
μ	fuzzy membership function
η	y/b
Γ	circulation
Λ	sweep angle
θ	geometry control variable

Abstract

The paper addresses an aerodynamic optimization methodology for obtaining an optimal wing geometry of wing/body configuration of regional jet aircraft. An adaptive optimization scheme is presented, in which optimization problems are solved sequentially to obtain the best design that meets given design criteria, by means of a combination of CFD analysis and design tools. Each optimization problem represents a subset of the design criteria, defining a subspace of physically feasible designs. The optimization results are evaluated, and if further improvements are deemed necessary, the optimization problem is adapted, such that a relatively well-posed optimization problem can be formulated in the final design cycles. To account for different levels of flow modeling that underly the CFD tools, a defect-correction procedure is applied. Results of three-dimensional and successive two-dimensional wing design optimizations are presented.

*Research Scientist, Computational Fluid Dynamics and Aeroelasticity Department, Fluid Dynamics Division, National Aerospace Laboratory NLR.
†Professor, Department of Aeronautics and Astronautics, Stanford University.
‡Research Engineer, Aeronautical Engineering, Empresa Brasileira de Aeronáutica S.A.
§Head, Fluid Dynamics Division, National Aerospace Laboratory NLR.
Copyright © 2001 by National Aerospace Laboratory NLR. Published by the American Institute of Aeronautics and Astronautics, Inc. with permission.

(c)2002 American Institute of Aeronautics & Astronautics or Published with Permission of Author(s) and/or Author(s)' Sponsoring Organization.

Introduction

The starting point of any detailed aircraft design is the specification of the design criteria in relation to the mission that the aircraft has to fulfill. The designer's task is not only to meet the specification with a minimum or at least acceptable risk, but also to provide an adequate level of competitiveness in his design product quality relative to any potential rival in the aircraft industry.

For the specific case of the regional aircraft market, the issue of competitiveness has grown very importantly during the past decade. The insertion of specifically designed regional jets has brought operational and comfort standards to a much higher level, compared to the typical regional turboprop aircraft from a previous generation. On the other hand, the level of performance requirements has been elevated, with time available for development considerably shortened due to an extremely demanding competition environment. As a result, the application of robust aerodynamic design techniques has become a factor of prime importance in the development of new generation regional jet aircraft, in order to attain the challenging mission requirements imposed by the market.

The mission is generally specified as a flight profile along which the aircraft has to perform, with the flight condition changing continuously. As dealing directly with the whole continuous mission profile is a formidable task, it is common practice to divide the profile into segments which are decisive for the overall quality of the design. For each individual segment, a design point and design criteria are specified, noting that properties on a design point cannot be isolated from those of the other design points.

In general, an aircraft has quite a complex geometry. It is practically impossible to handle the aircraft as a single entity during the detailed design phase. Hence, it is also common practice to decompose the aircraft into components having distinct functions and properties. To each component, a subset of the design criteria is assigned, taking into consideration that there are interactions between different components.

Another dimension of aircraft design problem is due to traditional classification into such disciplines as aerodynamics, structures, performance, stability and control. In this respect, the problem can be divided into a number of interrelated mono-disciplinary problems.

Although in the above approach, i.e. a priori subdividing a design problem into smaller subproblems, there is an inevitable risk of obtaining a design solution which is optimal only locally inside the domain of a subproblem,[1] significant payoffs can be gained from advances in analysis and synthesis methods within disciplines. Indeed, this line of thought has been followed in exploiting advances in Computational Fluid Dynamics (CFD) technology in aircraft design process.[2-5] The coupling between the subproblems can then be done by means of an iterative method.[6]

This paper addresses a CFD-based optimization methodology for wing design of a wing/body configuration of regional jet aircraft at design points associated with transonic flow conditions. The cross-sectional geometries of the wing are to be designed. The design criteria represent such goals as target fuel-tank volume, aerodynamic forces and moments coefficients, flow conditions, buffet-onset characteristics, and constraints which also incorporate multi-disciplinary aspects. Bearing in mind that design criteria specification is also a crucial step in a design process, this paper concentrates on the approach of solving optimization problems sequentially to obtain a best design that meets given design criteria, by means of a combination of CFD analysis and design tools.

In the optimization methodology, the design criteria must be formulated in a mathematical expression stating the optimization problem. The problem statement defines the objectives to be minimized and the constraints to be satisfied as functions of a vector of control (design) variables. Formulating the design criteria into a suitable set of objectives, constraints and control variables, and selecting the starting point of optimization, are not trivial tasks. The optimization problem formulation should lead to a design space, representing a subspace of physically feasible designs, that includes an optimum point corresponding to the best design. The selection of the starting point should imply a favorable path towards the optimum point to be found by the optimization algorithm.

In general, the human designer's knowledge on the relation between the design criteria, the optimization problem statement and the implied design space is limited. A new project generally implies a unique set of design criteria. Hence, initially an optimization problem statement is at best an educated guess on a mathematical expression of the design criteria. After examining the solution of an initial optimization problem, there should be a provision to modify the optimization problem for the next design cycle, based on the designer's experience and insight. The design process may then be considered as a learning process for the designer, to know the nature of the design criteria and to understand the relations between various design requirements, such that a relatively well-posed optimization problem can be formulated at the final design stages.

The optimization problem formulation is in-

(c)2002 American Institute of Aeronautics & Astronautics or Published with Permission of Author(s) and/or Author(s)' Sponsoring Organization.

evitably dependent on the CFD analysis and design optimization tools used, computational resources available, budget and time allocated. One should also be aware that the CFD analysis and design tools may have different levels of representation of the flow physics, and that there may be restrictions on the type of objectives and constraints, and flow conditions, that can be dealt with by the CFD tools. On the other hand, for a meaningful numerical optimization, the CFD analysis and design tools must also be of sufficient sophistication to facilitate timely and accurate examination by the designer.

In the present design exercise, a 3D analysis code MATRICS-V,[7] a 3D design code SYN88[8–10] and a 2D design code AEROPT[11,12] are applied during the design process. These codes are considered to represent the best combination, selected from the available CFD tools to ensure adequate design results obtained with short turn-around time between design cycles, as required by the industrial environment. Yet, this combination is considered to have a large potential to produce improved designs.

This paper is organized as follows. First, the design criteria are presented, followed by an explanation of the adaptive optimization scheme. The elements of the scheme are described in terms of the CFD analysis code, a generic form of optimization problem statement, and the CFD design codes. Computational results are then presented, demonstrating the effects of adapting optimization problem for multi-point transonic wing design, and finally conclusions are drawn in the last section.

Design Criteria Specification

Given a fixed wing planform, with the sweep angle and the area not to be altered, the geometries of the wing cross-sections are to be optimized:

- to achieve a minimum increase of 5.4% in the net fuel-tank volume,
- to maintain manufacturability and structural strength,

while at the same time:

- to improve the cruise performance (in terms of lift-to-drag ratio),
- to improve the off-design characteristics with respect to buffet-onset boundary,
- to satisfy a maximum nose-down pitching moment constraint in relation with maximum limits on the tail-load and the trim drag,
- to provide sufficient margins from trailing edge flow separation at low Reynolds numbers to allow wind tunnel testing,

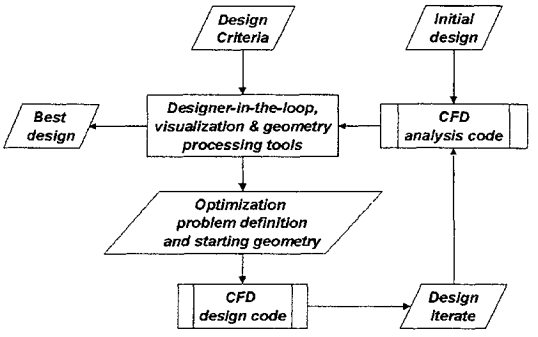

Fig. 1 Adaptive optimization scheme.

- to maintain adequate margins from supercritical velocities on the lower wing surface near the wing kink to take into account engine/airframe integration.

Adaptive Optimization Scheme

To formulate all requirements simultaneously into an optimization problem is a formidable task. The adaptive optimization strategy consists of design cycles, where in each cycle a subset of the design criteria is dealt with in order to understand the relations between various design requirements, while approaching the best design solution that fulfills the complete set of the design criteria.

Figure 1 depicts the process of adaptive optimization scheme. The scheme begins with the specified design criteria and an initial wing geometry of the wing/body configuration as an initial design iterate. The flow around this configuration is then calculated by means of a CFD analysis code. The designer, as man-in-the-loop, assesses the geometric properties and the flow characteristics with respect to the design criteria, using visualization and geometry processing tools. If further improvements are desired, a subset of the design criteria is identified, based on which the designer defines an initial optimization problem (or adapts a previous one).

The new optimization problem should be formulated as such that its solution would lead to the desired improvements. The designer decides whether the current design iterate or a variation thereof should be used as a starting point for the new optimization. The CFD design code performs the optimization, and the resulting optimal solution is treated as a new design iterate. The process is then repeated until the best design is obtained. It should be noted that in a larger design-loop the best design can be further assessed, which may lead to an adjustment of the design criteria.

(c)2002 American Institute of Aeronautics & Astronautics or Published with Permission of Author(s) and/or Author(s)' Sponsoring Organization.

For example, some variations of the wing planform may become allowable. However, this larger design-loop is beyond of the scope of this paper.

CFD Analysis Code

The CFD analysis code performs flow analyses of wing design iterates of the wing/body configuration to provide the flow solutions. A validated code should be used with sufficient capabilities to capture important flow characteristics. At the same time, as it will be used in an iterative design scheme, the analysis code should also provide a quick turn-around.

The MATRICS-V[7] code is employed to perform the flow analyses. The flow model is based on the full-potential flow in quasi-simultaneous interaction with boundary-layers on the wing, allowing considerable extent of flow separation to be modeled. To support the identification of possible wing design improvements, MATRICS-V gives a breakdown of the total drag into separate physical components:

- induced drag, produced by wing trailing edge vortex flow,
- viscous drag, originating from viscous stresses in boundary-layers and wakes,
- wave drag, resulting from losses associated with shock waves.

Spanwise distributions of these components of the total drag are presented such that wing sections that need to be improved can be identified conveniently. Also, other important aerodynamic characteristics, such as drag-divergence Mach number, buffet-onset boundary and boundary layer properties, are available from the flow analyses. Conditions that can lead to critical shock-induced and trailing-edge boundary layer separations are indicated by the growth of a three-dimensional boundary layer shape factor H.

Optimization Problem Statement

In order to apply the optimization methodology, the design criteria must be formulated as an optimization problem. A generic form of optimization problem statement can be expressed as

$$\begin{aligned} &\text{Minimize} && \mathcal{P}_{ij}(\mathbf{Q}_j, \mathbf{W}_j, \theta), \\ & && i = 1,..,n_p, \quad j = 1,..,n_f \\ &\text{Subject to:} \\ &\mathcal{A}_{kj}(\mathbf{Q}_j, \theta) \leq 0, && k = 1,..,n_a, \quad j = 1,..,n_f, \\ &\mathcal{G}_l(\theta) \leq 0, && l = 1,..,n_g, \end{aligned} \tag{1}$$

where θ is the control variables defining the wing cross-sectional geometries, $\mathbf{W}_j$ represents the parameters specifying the flow condition at a design point j, $\mathcal{P}_{ij}$ and $\mathcal{A}_{kj}$ refer to aerodynamic objective and constraint functionals, while $\mathcal{G}_l$ denotes geometric constraints. Multi-objective optimization problem is implied if $n_p > 1$. The total number of constraints consists of n_a aerodynamic constraints and n_g geometric constraints. Multi-point optimization is allowed by specifying $n_f > 1$ for the number of design points. In the adaptive optimization scheme, the dimensions of the optimization problem (n_a, n_g, n_p and n_f), the type of objectives and constraints ($\mathcal{P}$, $\mathcal{A}$ and $\mathcal{G}$), and the flow models may vary from one design cycle to another.

For given θ and $\mathbf{W}_j$, the values of the flow variables $\mathbf{Q}_j$ are obtained by solving the governing flow equations expressed in a conservative form as

$$\vec{\nabla} \cdot \vec{\mathbf{F}}_j(\mathbf{Q}_j, \mathbf{W}_j) = 0, \quad j = 1,..,n_f, \tag{2}$$

with $\vec{\mathbf{F}}$ the fluxes, subject to the boundary conditions

$$\mathbf{B}_j(\mathbf{Q}_j, \mathbf{W}_j, \theta) = 0, \quad j = 1,..,n_f. \tag{3}$$

CFD Design Code

The CFD design code performs optimization to find a new design iterate as a solution to the current optimization problem. While the algorithm of the CFD design code should be efficient, it should also incorporate the relevant flow physics, such that the geometric modifications produced will correspond to a new design that is closer to meeting the design criteria. An inviscid 3D design code SYN88[8–10] and a viscous 2D design code AEROPT[11,12] are used in parallel at various stages of the design process.

SYN88 provides an aerodynamic optimization tool for wing design of wing/body configurations in an inviscid flow governed by the Euler equations. A cell-centered finite-volume scheme is employed for space discretization of the Euler equations. Second-order dissipation terms are added to the fluxes of the flow equations for capturing the shock wave. The flow solutions are obtained through time integration towards a steady-state using an explicit Runge-Kutta scheme. For the stability of the time integration, fourth-order dissipation terms are added to the fluxes. As the optimization is performed in a three-dimensional inviscid flow domain, this code facilitates three-dimensional minimization of drag consisting of wave and vortex drag, subject to aerodynamic and geometric constraints.

AEROPT provides an aerodynamic optimization tool for airfoil design in a viscous flow governed by the Reynolds-Averaged Navier-Stokes equations with the Baldwin-Lomax algebraic turbulence model.[13,14] A cell-vertex finite-volume scheme is used for space discretization. Second-order dissipation terms are added to the fluxes of

(c)2002 American Institute of Aeronautics & Astronautics or Published with Permission of Author(s) and/or Author(s)' Sponsoring Organization.

the flow equations for capturing the shock wave. The flow solutions are obtained through time integration towards a steady-state using an explicit Runge-Kutta scheme. For the stability of the time integration, fourth-order dissipation terms are added to the fluxes. As the optimization is performed in a two-dimensional viscous flow domain, this code facilitates two-dimensional minimization of sectional drag consisting of the viscous and wave drag components, subject to aerodynamic and geometric constraints.

Both design codes employ gradient-based optimization algorithms. The variational method is applied for efficient computations of the gradients through solutions of continuous adjoint equations, obtained with the same numerical scheme used for solving the flow equations. A general form of aerodynamic functionals is considered as follows,

$$\mathcal{F} = \int_{S_w} \psi(\mathbf{Q}, \mathbf{W}, \theta)\, dS \tag{4}$$

where the notation $\mathcal{F}$ applies for both $\mathcal{P}$ and $\mathcal{A}$, while S_w is the surface of the aerodynamic shape to be optimized. ψ is a local functional representing a large class of aerodynamic goals, including those expressed in terms of lift, drag, and pitching moment coefficients. For each pair of an aerodynamic functional and a design point (specified by a constant value of $\mathbf{W}$), a Lagrangian is defined as

$$\begin{aligned} \mathcal{L} &= \int_{S_w} \psi(\mathbf{Q}, \mathbf{W}, \theta)\, dS \\ &+ \int_{\Omega} \boldsymbol{\lambda} \cdot (\vec{\nabla} \cdot \vec{\mathbf{F}}(\mathbf{Q}, \mathbf{W}))\, d\Omega \\ &+ \int_{S_w} \boldsymbol{\Upsilon} \cdot \mathbf{B}(\mathbf{Q}, \mathbf{W}, \theta)\, dS, \end{aligned} \tag{5}$$

where $\boldsymbol{\lambda}$ is the so-called vector of adjoint variables, $\boldsymbol{\Upsilon}$ is the vector of Lagrange multipliers associated with the boundary conditions, and Ω is the flow domain. The variation of the Lagrangian is evaluated as

$$\delta\mathcal{L} = \delta\mathcal{L}_\lambda + \delta\mathcal{L}_\Upsilon + \delta\mathcal{L}_Q + \delta\mathcal{L}_\theta, \tag{6}$$

where $\delta\mathcal{L}_\lambda$ refers to the variation of $\mathcal{L}$ due to the variation of $\boldsymbol{\lambda}$ while the other variables are kept fixed, and similarly for the other terms. The variational method consists of a procedure for setting the variations $\delta\mathcal{L}_\lambda$, $\delta\mathcal{L}_\Upsilon$ and $\delta\mathcal{L}_Q$ equal to zero. Setting $\delta\mathcal{L}_\lambda = 0$ and $\delta\mathcal{L}_\Upsilon = 0$ is equivalent with satisfying the flow equations and the boundary conditions, providing the values of the flow variables $\mathbf{Q}$. Setting $\delta\mathcal{L}_Q = 0$ leads to a set of adjoint equations and boundary conditions, the solution of which provide the values of the adjoint variables $\boldsymbol{\lambda}$ and the Lagrange multipliers $\boldsymbol{\Upsilon}$. The variation $\delta\mathcal{L}$ becomes

$$\delta\mathcal{L} = \delta\mathcal{L}_\theta, \tag{7}$$

from which an expression for gradient of the aerodynamic functional $\mathcal{F}$ with respect to θ can be obtained. The gradient information is passed on to the optimization algorithm. The computational effort of solving the adjoint equations is comparable to that of solving the flow equations. Thus, the computational effort of obtaining the gradient is about twice that of solving the flow equations, irrespective of the dimension of the control variables. This feature is important because it gives the designer a large flexibility in formulating the optimization problem.

It should now be noted that, from the 3D viscous flow model of MATRICS-V, the viscous effects are missing in the 3D inviscid flow model of SYN88, while the three-dimensional effects are missing in the 2D viscous flow model of AEROPT. Because the flow modeling underlying the CFD design codes are less complete than that underlying the CFD analysis code, the optimization must be performed in a defect-correction fashion as follows.

An evaluation of a current design iterate gives the pressure distribution over the wing surface. This process is symbolized as

$$C_p = N\theta, \tag{8}$$

where C_p represents the pressure coefficient distribution, N is an operator representing the flow analysis using the more complete flow model, and θ refers to the current wing geometry. Now, an operator $\widetilde{N}$ is introduced for the flow analysis using the less complete flow model underlying the design code. An inverse procedure, defined as

$$\tilde{\theta} = \widetilde{N}^{-1} C_p, \tag{9}$$

is performed to obtain a geometry $\tilde{\theta}$. In the less complete flow model, this geometry produces a pressure distribution $\widetilde{C}_p$,

$$\widetilde{C}_p = \widetilde{N}\tilde{\theta}. \tag{10}$$

where $\widetilde{C}_p$ approximates C_p following a condition that $\|\widetilde{C}_p - C_p\|^2$ is minimum. In this approximate sense, the geometry $\tilde{\theta}$ can be interpreted as

$$\tilde{\theta} = \theta + \delta\theta, \tag{11}$$

where $\delta\theta$ is a geometric correction that incorporates the missing flow physics. An operator $\mathcal{M}$ is introduced for optimization using the less complete flow model, taking $\tilde{\theta}$ as the starting geometry while assuming $\delta\theta$ constant. The optimization results in a new geometry $\tilde{\theta}^*$:

$$\tilde{\theta}^* = \mathcal{M}\tilde{\theta}. \tag{12}$$

Because $\delta\theta$ is assumed constant, the geometry $\tilde{\theta}^*$ can also be interpreted as

$$\tilde{\theta}^* = \theta^* + \delta\theta, \tag{13}$$

(c)2002 American Institute of Aeronautics & Astronautics or Published with Permission of Author(s) and/or Author(s)' Sponsoring Organization.

where θ^* represents an actual geometry in the more complete flow model. The new design iterate θ^* can be determined from

$$\theta^* = \theta + \omega(\tilde{\theta}^* - \tilde{\theta}), \tag{14}$$

with ω a relaxation factor. A subsequent evaluation of the new design iterate provides a new pressure distribution C_p^*,

$$C_p^* = N\theta^*. \tag{15}$$

If the examination of C_p^* and θ^* by the designer still suggests further improvement, then the problem statement is updated accordingly, and the process is repeated for the next design cycle with the new optimization problem.

N in the above scheme represents MATRICS-V that solves the full-potential equations with the boundary layer equations on the wing in a three-dimensional domain around the wing/body configuration. $\tilde{N}$ represents AEROPT (SYN88) that solves the two-dimensional RANS (three-dimensional Euler) equations, while the symbols $\tilde{\theta}$ and $\delta\theta$ refer to two-dimensional airfoil shapes (three-dimensional wing shapes), p and $\tilde{p}$ are local cross-sectional (surface wing) pressure distributions, and $\mathcal{M}$ is an operator for constrained multi-point aerodynamic optimization of airfoils (wings of the wing/body configuration).

Computational Results

MATRICS-V and AEROPT were executed on the National Aerospace Laboratory's NEC SX-5 supercomputer in the Netherlands, while SYN88 was executed on a Pentium-based computer at Stanford University in the United States. 3D and 2D optimizations were performed in parallel at the two sites. Internet technology has been exploited for communication and data exchange. It was experienced that the 10-hour time difference between the two geographical locations could shorten the elapsed time of consecutive design cycles. For example, computational results of an 8-hour long design run that finished around midnight at one site could be assessed immediately by the designer at the other site, which in turn could adapt the problem and submit a new design run.

Starting from an infeasible fuel tank volume, it became soon obvious during the design process that the minimum 5.4% increase of fuel volume in combination with the fixed wing planform was demanding. This combination seems to imply a narrow feasible design space for aerodynamic optimization aimed at cruise performance and off-design characteristics with adequate margins to trailing edge flow separation and supercritical velocities on the lower surface.

The design exercise produced 17 different wings, resulting from 2D and 3D design cycles with different sets of objectives and constraints. Quantitatively, in terms of the fuel tank volume and aerodynamic coefficients, the results of 2D and 3D optimizations are comparable. The best design has been determined based also on the qualitative aspects, such as the characteristics of the pressure distribution, expected buffet-onset properties, and the risks related to wind tunnel testing and engine/airframe integration.

The best design, resulting from the two-dimensional optimizations, represents 6.7% increase in the fuel volume (larger than the minimum target). The cruise performance has been enhanced, with 57% reduction of wave drag, 1.4% increase in viscous drag and practically unchanged vortex drag, giving a net reduction of 2 drag counts. The margin to buffet-onset boundary is enlarged by 1.5% in terms of C_L. Other constraints considering the tail-load and trim drag (maximum nose-down pitching moment), wind tunnel testing (attached flow at low Reynolds number), and engine/airframe integration (maximum velocities on the lower surface) are satisfied. Wind tunnel testing has been performed, and the results verified the outcome of the design exercise.

Some design cycles are less successful than the other ones, but these cycles provide valuable information to adapt the optimization. Only a few design cycles will be discussed here, bearing in mind that the other cycles were also important steps in the adaptive optimization strategy. The results to be presented are limited to those of consecutive design cycles demonstrating the effect of adapting an optimization problem.

The defect-correction approach explained in the previous section is followed. Both design codes have the capability of performing an inverse shape design through minimizing a functional of the type

$$\mathcal{F}_{inverse} = \int_{S_w} \frac{1}{2}(\tilde{p} - p)^2 \, dS. \tag{16}$$

The operator $\tilde{N}^{-1}$ in equation (9) represents the algorithm to minimize the functional (16) employed by the design codes to yield a geometry $\tilde{\theta}$.

3D Optimization

A wing geometry θ of a current design iterate is considered. A viscous flow analysis using MATRICS-V is performed for this geometry and, after an evaluation, further improvements are deemed necessary through global modification of the wing surface. Figure 2 shows distributions of the pressure coefficient at an inner and a near-kink wing station. $C_p(\theta)$ (indicated by circles) is the viscous pressure distribution computed by

(c)2002 American Institute of Aeronautics & Astronautics or Published with Permission of Author(s) and/or Author(s)' Sponsoring Organization.

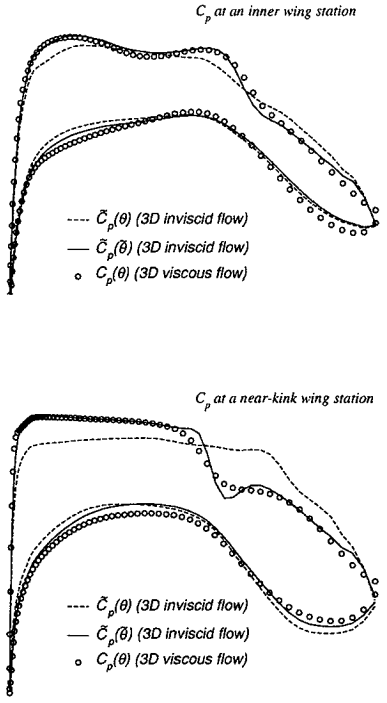

Fig. 2 3D inverse design.

MATRICS-V for a current wing design iterate at the cruise design point. For the same geometry and the same flow condition (also the same C_L), the solution of the Euler equations gives $\widetilde{C}_p(\theta)$ (dashed lines), obtained by the analysis mode of SYN88. The difference between $C_p(\theta)$ and $\widetilde{C}_p(\theta)$ gives an idea about the viscous effects due to the boundary layer displacement, which in this case are clearly significant.

Applying the inverse mode of SYN88 with $C_p(\theta)$ as the target yields a geometry $\tilde{\theta}$. The figure shows that some discrepancies are still visible between the obtained $\widetilde{C}_p(\tilde{\theta})$ and the target $C_p(\theta)$, in particular near the shock wave. This may be attributed to the fact that the inviscid flow model produces sharp shock waves and therefore cannot match the pressure of the shock wave boundary layer interaction with the lower gradient. Nevertheless, the pressure distributions shown represent a minimum deviation in the sense of (16), such that the geometry $\tilde{\theta}$ may be considered as incorporating the viscous effects in the inviscid flow domain around the wing/body configuration.

A 3-point constrained drag optimization problem is stated as follows:

$$\begin{aligned} &\text{minimize} && w_1 C_{D_1} + w_2 C_{D_2} + w_3 C_{D_3}, \\ &\text{subject to:} \\ &\quad t/c_{max} && \geq \; t/c_{max,initial}, \end{aligned} \tag{17}$$

where the subscripts 1, 2, and 3 indicate the three design points specified by the lift coefficients and

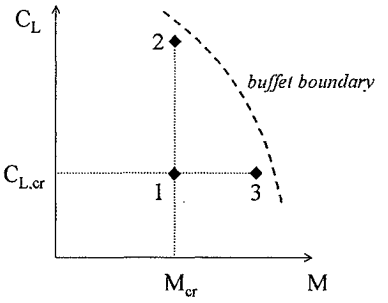

Fig. 3 Design points in 3D optimization.

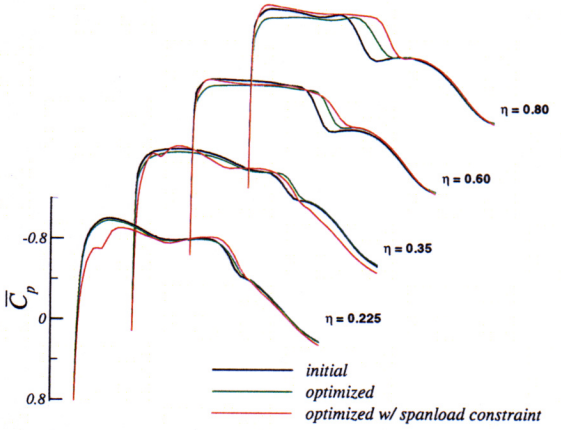

Fig. 4 Results of 3D optimizations.

Mach numbers depicted in Figure 3. It should be noted that for all design points the fixed C_L values are implicitly satisfied together with the solutions of the Euler equations. The objective to be minimized is a weighted sum of drag coefficients at these design points. It is expected that, while trying to minimize the drag at the cruise condition, minimizing the drag at the second and third design points would weaken the shock waves at conditions near the buffet-onset boundary, such that the shock-induced boundary layer separation would be delayed. The purpose of the maximum thickness constraint is to maintain the fuel volume currently representing 5% increase from that of the baseline.

The geometry $\tilde{\theta}$ obtained from the above inverse procedure is taken as the starting geometry. The optimization using SYN88 yields a geometry $\tilde{\theta}^*$, for which the thickness constraint is actively satisfied. The drag coefficients at the three design points in the inviscid flow have been reduced significantly, while the new inviscid pressure distributions indicate weaker shock waves.

The actual geometry θ^* is obtained through equation (14), which is subsequently evaluated using MATRICS-V. Figure 4 shows the upper surface pressure distributions ($\bar{C}_p$) before (black) and after (green) the optimization. The new pressure distribution indicates reduction of the shock wave

(c)2002 American Institute of Aeronautics & Astronautics or Published with Permission of Author(s) and/or Author(s)' Sponsoring Organization.

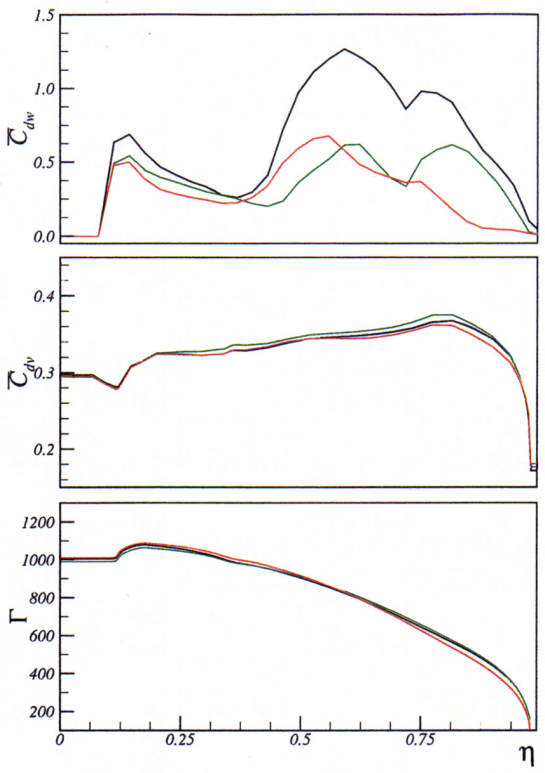

Fig. 5 Results of 3D optimizations.

strength, leading to a lower wave drag. Figure 5 shows spanwise distributions of the sectional wave drag ($\bar{C}_{dw}$), viscous drag ($\bar{C}_{dv}$) and circulation (Γ), normalized with respect to the respective initial integrated values. The sectional wave drag is reduced along the span, and more significantly on the outer wing stations, giving 40% reduction of the wave drag. The new geometry produces higher sectional viscous drag. It is observed that downstream of the shock wave there is a rapid growth of the boundary layer, which explains the higher viscous drag (0.6% increase in the viscous drag). The circulation distribution is slightly pushed towards an elliptical distribution, giving 1% reduction of the vortex drag.

A control over the spanwise load distribution is considered necessary to obtain a more triangular distribution, which is expected to yield: (i) reduced nose-down pitching moment implying smaller trim drag and tail-load, (ii) delayed buffet-onset and less sectional viscous drag on the outer wing, and also (iii) less root bending moment potential for weight reduction.

The optimization problem is adapted by introducing an equality constraint of the form:

$$C_l(\eta) = C_{l_t}(\eta), \quad 0 \le \eta \le 1, \tag{18}$$

where C_{l_t} is the desired distribution. It should be noted that this constraint is applied in the inviscid flow, as the optimization is still performed by SYN88, meaning that an equality constraint on the spanwise load in the inviscid flow does not necessarily imply the same spanwise load in the viscous flow.

The new results are indicated in red in the above figures, where the effect of the constraint is evident. A significant amount of twist (in the wash-out orientation) has been introduced by the optimization algorithm. This provides a lower sectional angle of attack on the outer wing, giving a lower sectional lift implying lower wave drag and viscous drag. On the other hand, a significant increase in the velocity is observed on the lower surface, which may not be favorable for engine/airframe integration. The more triangular distribution results in a slight increase of the vortex drag, but this is compensated by significant gains from the reductions of both wave and viscous drag. Relative to the initial values (black), 46% wave drag and 0.2% viscous drag reductions have been achieved, with no noticeable change in the vortex drag.

2D optimization

A wing geometry θ of a current design iterate is considered. A viscous flow analysis using MATRICS-V is performed for this geometry and, after an evaluation, further improvements are deemed necessary through local modifications of the wing sections.

In order to perform a meaningful two-dimensional optimization, three-dimensional effects must be incorporated in the two-dimensional domain. As a first approximation, the simple-sweep theory is applied. The flow condition (Mach and Reynolds numbers), the local sectional viscous pressure distribution given by MATRICS-V, and the geometry are scaled as follows,

$$M_s = M_\infty cos\Lambda, \tag{19}$$
$$\mathrm{Re}_s = \mathrm{Re}_\infty cos^{-2}\Lambda, \tag{20}$$
$$C_{p_s}(\theta) = C_p(\theta) cos^{-2}\Lambda, \tag{21}$$
$$t/c(\theta_s) = t/c(\theta) cos\Lambda, \tag{22}$$

where Λ is the sweep-angle taken along the wing quarter-chord. $C_p(\theta)$ is the sectional distribution given by MATRICS-V for the current wing design iterate. The last expression is the scaling of the thickness of the sectional geometry θ. Figure 6 shows $\widetilde{C}_p(\theta_s)$ (dashed-line) obtained using the two-dimensional viscous flow model at the scaled geometry and scaled flow condition. There is still a significant deviation between $C_{p_s}(\theta)$ and $\widetilde{C}_p(\theta_s)$, which means that the simple-sweep theory does not sufficiently incorporate the three-dimensional effects. The finite wing span, and the spanwise variations of the chord and the airfoil shape, must have contributed to the three-dimensional effects not modeled by the simple-sweep theory.

(c)2002 American Institute of Aeronautics & Astronautics or Published with Permission of Author(s) and/or Author(s)' Sponsoring Organization.

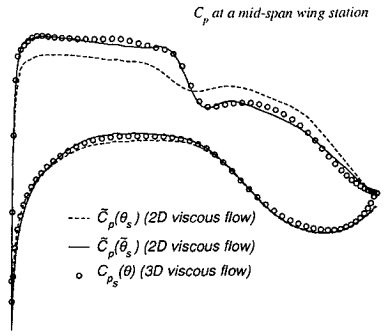

Fig. 6 2D inverse design.

An inverse procedure using AEROPT is then performed, with $C_{p_s}(\theta)$ as the target and θ_s as the starting geometry. The results is a geometry $\tilde{\theta}_s$ which produces $\tilde{C}_p(\tilde{\theta}_s)$ in the two-dimensional viscous flow domain. Figure 6 shows that $\tilde{C}_p(\tilde{\theta}_s)$ closely recovers the target $C_{p_s}(\theta)$. In this sense, the geometry $\tilde{\theta}_s$ may be considered as incorporating the three-dimensional effects.

Three defining wing sections are considered, located at an inner, an outer, and a kink area of the wing. The wing surface is defined by interpolation between these sections. Three successive design cycles are performed. The first cycle is aimed at optimizing the inner section. In the second cycle, after evaluation of the new viscous flow solution obtained from the first cycle, the outer section is optimized. Finally, based on the outcome of the second cycle, an optimization problem for the kink section is formulated and solved.

In these design cycles, the aerodynamic design problems are formulated as multi-objective fuzzy optimization problems,[15] which can be expressed in a general form as follows,

$$\text{Maximize} \quad min(\mu_i(C_{d_i})), \quad i = 1,..,4 \tag{23}$$

Subject to:

$$C_{m_1} \geq C_{m_1} \tag{24}$$

$$A_{fuel} \geq A_{fuel,initial}, \tag{25}$$

$$R_{LE} \geq R_{LE,initial}, \tag{26}$$

$$\delta_{TE} \geq \delta_{TE,initial}, \tag{27}$$

$$t/c_{0.75c} \geq t/c_{0.75c}. \tag{28}$$

The subscript i refers to four design points illustrated in Figure 7. The flow solution procedure is performed in the fixed C_l mode. Design point 1 corresponds to the cruise condition. Design points 2 and 3 are associated with conditions near the buffet-onset boundary. Design point 4 is included to suppress the tendency of a singular behavior of optimal solution at the cruise design point. This refers to a situation in which a very low drag value is typically achieved precisely at the cruise condition, but high drag values occur at conditions slightly different from that of the cruise condition.

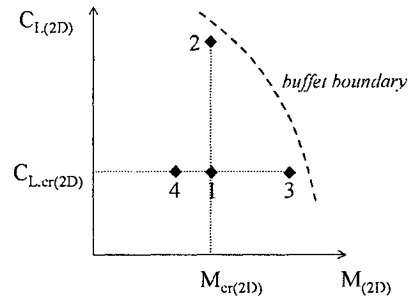

Fig. 7 Design points in 2D optimization.

In fuzzy optimization, an objective is expressed in terms of a monotone function μ, $0 \leq \mu \leq 1$, referred to as the membership function. An objective value giving $\mu = 1$ is considered most satisfactory, while $\mu = 0$ indicates a very undesirable value of the objective. Thus, for a (*bad*) high drag situation, a value close to zero is assigned to $\mu(C_d)$, while a (*good*) low drag situation corresponds to a value of $\mu(C_d)$ close to one. This formulation provides a natural way of adapting the optimization problem, as the designer is expected to have a good idea about bad or good values that should be achieved or avoided after evaluating a current design iterate.

Constraint (24) is an aerodynamic constraint that limits the nose-down pitching moment at cruise. Constraint (25) maintains the fuel tank volume currently representing a 6.7% increase relative to that of the baseline wing. Constraint (26) limits the leading edge radius for low-speed stall consideration. Constraint (27) in combination with constraint (28) take into account aspects of manufacturability and structural strength, by avoiding geometries with excessively thin trailing edge region.

Figures 8 and 9 present the pressure distributions ($\bar{C}_p$) and spanwise distributions of the sectional wave drag ($\bar{C}_{dw}$), viscous drag ($\bar{C}_{dv}$) and circulation (Γ), before (black) and after optimization of the inner-section (blue), outer-section (green) and kink-section (red). From the pressure distributions, it can be observed that optimization of the inner-section has quite a local effect, i.e. in the outer stations ($\eta = 0.60$ and $\eta = 0.80$) the blue curves overwrite almost completely the black (initial) curves. The same applies to optimization of the outer-section, where the green curves almost totally overwrite the blue curves in the inner stations ($\eta = 0.225$ and $\eta = 0.35$).

The outcome of the first design cycle (inner-section optimization) can be identified as: higher suction peak near the leading edge, slightly more

(c)2002 American Institute of Aeronautics & Astronautics or Published with Permission of Author(s) and/or Author(s)' Sponsoring Organization.

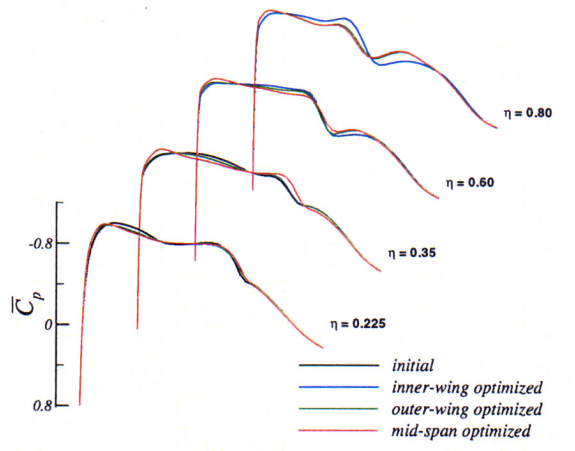

Fig. 8 Pressure distributions of 2D optimization results.

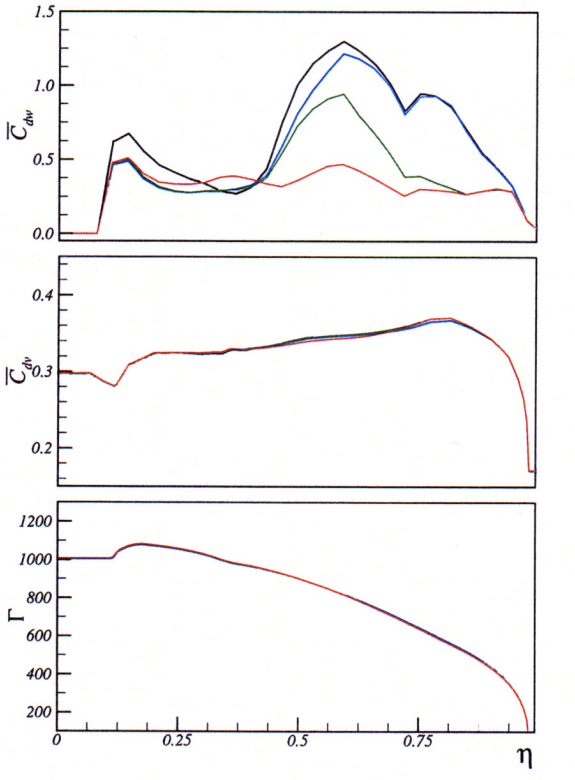

Fig. 9 Spanwise characteristics of 2D optimization results.

aft-loading, and lower sectional wave drag in the inner stations which is also indicated by more gentle gradient near the shock wave. There are no significant effects on the sectional viscous drag and spanwise load distributions.

The outcome of the second design cycle (outer-section optimization) can be identified as: higher suction peak near the leading edge, more gentle gradient near the shock wave, sloping roof-top pressure distribution, and a rather strong re-acceleration of the flow after the shock wave. The sectional wave drag in the outer stations have been reduced significantly. There is a noticeable increase of the sectional viscous drag at the outer stations, which can be related with a stronger growth of the boundary layer towards the trailing edge. The spanwise load distribution remains the same.

The third design cycle (kink-section optimization) is targeted at reduction of the sectional wave drag in the mid-span area. This optimization affects both the inner and outer wing areas. Along the span, higher suction peak near the leading edge and more sloping roof-top type of pressure distribution are observed. The strong re-acceleration flow in the outer station is alleviated, while the pressure gradient clearly indicates weaker shock waves. The sectional wave drag in the mid-span area has successfully been reduced, at the expense of a slight increase of the wave drag in the inner part of the wing. The wave drag becomes almost uniformly distributed along the span. The spanwise load distribution remains practically the same. In the inner stations, there is a remarkable reduction of the viscous drag.

Higher sectional viscous drag can be attributed to a stronger growth of the boundary layer towards the trailing edge. This type of flow is susceptible to trailing edge separation, especially in low Reynolds numbers like those occur in the wind tunnel. This stronger boundary layer growth is due to a region with high surface curvatures. These transonic bumps are known to be physical mechanisms, which are apparently recognized by the optimization algorithm, to weaken shock waves. To cope with this situation, a constraint of the form

$$C(x/c) \leq C_{max}, \quad 0.50 \leq x/c \leq 0.98 \qquad (29)$$

is introduced to limit the upper surface curvatures behind the shock wave. The effect of the constraint at $\eta = 0.60$ can be observed in Figure 10. The lower picture shows that, after the curvature constraint is applied, less growth of the boundary layer shape factor H is achieved, giving a significantly lower value of H at the trailing edge, thus providing sufficient margin to trailing edge separation. Remarkably, the curvature constraint did not contradict the reduction of wave drag, as even a lower wave drag was achieved. The pressure distribution appears to have adapted itself, by transferring a slight amount of the aft-load towards the middle part by slightly moving the shock wave aft, to allow a more gentle deceleration of the flow towards the trailing edge.

Another example from 2D optimization concerns a constraint on the lower wing surface of a wing section at the kink area. This constraint can be introduced to control the velocity on the lower surface indirectly. Allowing the the lower surface to move downward would shift the fuel-tank volume to the lower part, and therefore would provide

(c)2002 American Institute of Aeronautics & Astronautics or Published with Permission of Author(s) and/or Author(s)' Sponsoring Organization.

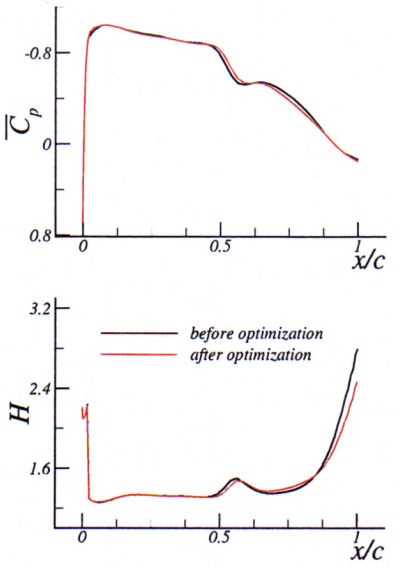

Fig. 10 Upper surface $\bar{C}_p$ and H distributions at $\eta = 0.60$.

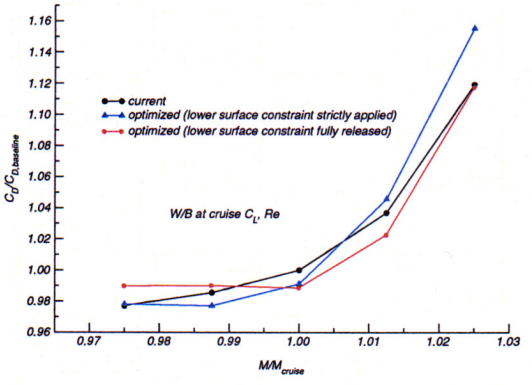

Fig. 11 Effect of lower surface constraint to drag rise.

some flexibility for streamlining the upper surface. As a consequence, bringing the volume towards the lower part may imply higher velocity on the lower surface, thus may give additional risks with respect to airframe/engine integration. Figure 11 gives an idea of the possibilities that can be obtained by using such a control within optimization. While the improvements of the cruise performance are practically the same, the properties below and above the cruise Mach number are significantly different, representing conflicting characteristics: potentially higher drag-divergence Mach number but higher drag at lower Mach numbers and larger risks on airframe/engine integration (the lower surface velocity has become supersonic), against lower drag at lower Mach numbers and less risks on airframe/engine integration but possibly lower drag-divergence Mach.

Conclusions

An adaptive optimization strategy applied to wing design of a wing/body configuration of regional jet aircraft has been described. The design criteria have been met by successive optimization stages, where on each stage a subset of the design criteria is dealt with. The adaptive strategy allows one to understand the relations between various design requirements to approach the best design solution. The optimization results shown emphasize that obtaining an optimal design space, through a well-posed optimization problem, is a prerequisite to achieving the best design solution meeting all the design criteria.

A combination of CFD tools, consisting of a 3D viscous analysis code based on full-potential and boundary layer equations, a 3D inviscid design code based on the Euler equations, and a 2D viscous design code based on the RANS equations, has been used in the optimization process. A defect-correction approach has been applied, such that this combination with different levels of flow modeling leads to an actual design improvement in the flow model with the highest representation of the flow physics involved (three-dimensional viscous flow). However, it should be noted that a better perspective for the future may be given by a common high fidelity modeling, such as that provided by three-dimensional RANS equations, for the analysis and design (adjoint) codes.

The results of 3D and 2D optimizations are comparable quantitatively in terms of global geometric properties and aerodynamic coefficients. In the end, the best design is determined based also on qualitative aspects such as characteristics of the pressure distribution, expected buffet-onset properties and risks related to engine/airframe integration and wind tunnel testing.

Transonic wind tunnel tests have been performed at the DNW-HST in Amsterdam, conforming that the results from the present design exercise have led to the full attainment of cruise performance requirements for a new regional jet aircraft. From an industrial standpoint, the design methodology has proven to be sufficiently robust for solving real-life industrial design problems.

References

[1]Liddel, P., "Technical Evaluation Report," *Aerodynamic design and optimisation of flight vehicles in a concurrent multi-disciplinary environment*, RTO-MP-35, 2000.

[2]Jameson, A. and Vassberg, J., "Computational Fluid Dynamics for Aerodynamic Design: Its Current and Future Impact," *AIAA Paper 2001-0538*, 2001.

[3]Nielsen, E. and Anderson, W., "Recent improvements in aerodynamic design optimization on unstructured meshes," *AIAA Paper 2001-0596*, 2001.

[4]Soemarwoto, B., Labrujère, T., Laban, M., and Yansyah, H., "Inverse Aerodynamic Shape Design for Improved

(c)2002 American Institute of Aeronautics & Astronautics or Published with Permission of Author(s) and/or Author(s)' Sponsoring Organization.

Wing Buffet-Onset Performance," *Inverse Problems in Engineering Mechanics II*, edited by M. Tanaka and G. Dulikravich, Elsevier, 2000.

[5]Soemarwoto, B., "Airfoil optimization using the Navier-Stokes equations by means of the variational method," *AIAA Paper 98-2401*, 1998.

[6]Arian, E., *Convergence Estimates for Multidisciplinary Analysis and Optimization*, ICASE Rep. 97-57, 1997.

[7]van der Wees, A., van Muijden, J., and van der Vooren, J., *A fast and robust viscous-inviscid interaction solver for transonic flow about wing/body configurations on the bases of full potential theory*, NLR-TP-93214 U, 1993.

[8]Jameson, A., "Optimum Aerodynamic Design Using Control Theory," *CFD Review*, 1995, pp. 495–528.

[9]Reuther, J. and Jameson, A., "Aerodynamic Shape Optimization of Wing and Wing-Body Configurations Using Control Theory," *AIAA Paper 95-0123*, 1995.

[10]Jameson, A., Alonso, J., Reuther, J., Martinelli, L., and Vassberg, J., "Aerodynamic shape optimization techniques based on control theory," *AIAA Paper 98-2538*, 1998.

[11]Soemarwoto, B., *Multi-Point Aerodynamic Design by Optimization*, Ph.D. thesis, Delft University of Technology, also NLR TR 96534 L, 1996.

[12]Soemarwoto, B., *The Variational Method for Aerodynamic Optimization using the Navier-Stokes Equations*, ICASE Rep. 97-71/NASA CR-97-206277, 1997.

[13]Brandsma, F., "Description of the Method Used by NLR," *EUROVAL–A European Initiative on Validation of CFD Codes*, edited by H. W. *et.al*, Vol. 42 of *Notes on Numerical Fluid Mechanics*, Vieweg, Brunswick, 1993.

[14]Hagmeijer, R., "Grid Adaption Based on Modified Anisotropic Diffusion Equations Formulated in the Parametric Domain," *J. of Computational Physics*, Vol. 115, No. 1, Nov 1994, pp. 169–183.

[15]Soemarwoto, B. and Labrujère, T. E., "Airfoil design and optimization methods: recent progress at NLR," *Intl. J. Numer. Meth. Fluids*, Vol. 30, 1999, pp. 217–228.